ACS OMEGA

http://pubs.acs.org/journal/acsodf

Article

Temperature- and Composition-Induced Multiarchitectural Transitions in the Catanionic System of a Conventional Surfactant and a Surface-Active Ionic Liquid

Mohd Sajid Lone, Saima Afzal, Oyais Ahmad Chat, Vinod Kumar Aswal, and Aijaz Ahmad Dar*

Cite This: *ACS Omega* 2021, 6, 11974−11987

Read Online

ACCESS | Metrics & More | Article Recommendations | Supporting Information

ABSTRACT: The mixture of the cationic surfactant, cetyltrimethylammonium bromide (CTAB), and anionic surface-active ionic liquid, 1-butyl-3-methylimidazoliumdodecyl sulfate (bmimDS), has been studied as a function of the mole fraction of CTAB, X_{CTAB}, with the total surfactant concentration fixed at 50 mM using turbidity measurements, rheology, dynamic light scattering, differential scanning calorimetry, small-angle neutron scattering, and small-angle X-ray scattering techniques. The catanionic mixture has been found to exhibit phase transitions from vesicles to micelles as a function of temperature, with some mole fractions of CTAB showing dual transitions. Solutions of X_{CTAB} = 0.2 to 0.5 exhibited a single transition from vesicles to cylindrical micelles at 45 °C. With an increase in the mole fraction of CTAB from 0.55 to 0.65, dual structural transitions at 30 and 45 °C were observed. The microstructural transition at 30 °C is ascribed to the vesicle aggregation process with smaller vesicles fusing into bigger ones, whereas the transition at 45 °C was evaluated to be the vesicle-to-cylindrical micelle transition. However, at higher mole fractions of CTAB, X_{CTAB} from 0.65 to 0.90, a single transition from vesicles to small cylindrical/spherical micelles was observed in the solutions, at a lower temperature of 30 °C. To the best of our knowledge, such a microstructural transitions as a function of temperature in a single mixture of cationic and anionic surfactants without any additive has not been reported so far.

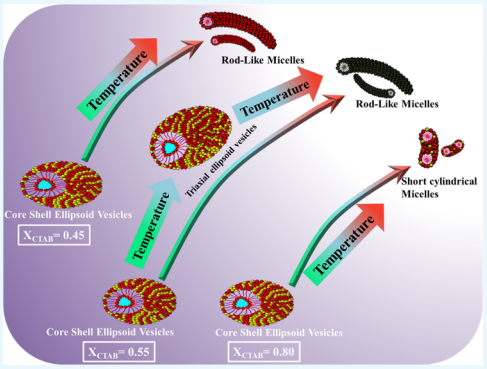

1. INTRODUCTION

Being one of the most significant soft materials, surfactant micellar systems have always been an interesting area of research due to their ability to self-assemble into well-defined microstructures of various shapes in the solutions.[1,2] The molecular interactions within these self-assemblies govern the phase behavior, resulting in the formation of a variety of microstructures such as spherical micelles, rodlike micelles, unilamellar vesicles, lamellar structures, and so forth.[3] Such microstructures possess distinct physicochemical properties and thus have been utilized in a plethora of applications ranging from the formulation of drug delivery vehicles to the synthesis of nanoparticles.[4,5] It is well documented in the literature that mixed surfactant systems are more expedient than their constituent surfactants due to the synergetic effect in their interfacial and self-assembly properties.[6,7] The mixture of cationic and anionic surfactants (catanionic mixture) presents an interesting soft system with remarkable features arising from the electrostatic interactions between the oppositely charged surfactants, leading to the formation of ion pairs with extremely high surface activity.[8,9] Such ion pairs have the remarkable tendency to form vesicles, structures with a bilayer of surfactant molecules enclosing a pool of water within them[10] having widespread applications ranging from synthetic templates to protein binders[11] to transfection vectors.[12] The vesicle forming ability of catanionic surfactants is a function of various factors, viz., the nature of the mixing surfactants, the addition of various alcohol additives, the presence of salts, and so forth.[13−15]

The exploration of stimuli-responsive microstructural transitions of the catanionic surfactant mixtures has been the focus of researchers in recent years. The tuning and control of microstructural evolution w.r.t. various external stimuli such as pH, temperature, light, salt, hydrotrope, and so forth[14−16] provide a variety of strategies to design the systems for desired properties.[17,18] As such, the microstructural transition between micelles and vesicles, being two important classes of self-assembled soft systems,[19] as a function of external stimuli has gained utmost importance and desirability. These transitions are of great interest in the biological and colloidal processes such as in the reconstitution of the membrane proteins and the

Received: January 26, 2021
Accepted: April 15, 2021
Published: April 27, 2021

release of drugs.[20] Sodium dodecylsulfate (SDS) and cetyltrimethylammonium bromide (CTAB) have been used mostly in such studies[14] to evaluate the effect of temperature, composition, salt, organic additives, and so forth on the microstructural transitions of their self-assembled aggregates. Temperature is the most easily controllable stimulus to realize the thermo-responsive microstructural transitions such as micelle-to-vesicle transition (MVT), vesicle-to-micelle transition (VMT), or vesicle-to-aggregated vesicle transition.[14,21,22] Recently, Rajkhowa et al.[14] have evaluated the effect of temperature, composition, and alcohol on the microstructures of SDS and CTAB in which they have observed both the types of transitions, MVT and VMT depending on the mole fraction of SDS. Earlier, Davies et al.[19] reported the microstructural transitions from vesicles to wormlike micelles upon heating in the mixture of CTAB and 5-methyl salicylic acid (5 mS), which was ascribed to the intercalation of 5 mS between the head groups of CTAB micelles. Majhi and Blume[23] have shown the temperature-induced MVTs in a mixture of dimyristoylphosphatidylcholine (DMPC)-sodium dodecyl sulfate (SDS) and DMPC-dodecyltrimethylammonium bromide (DTAB) wherein temperature plays a significant role, apart from concentration, to induce the MVTs. It is pertinent to mention here that some studies have reported the aggregation/growth of vesicles, rather than the usual MVTs or VMTs, with the increase in temperature that is considered as the possible route to frame the analogous models for better understanding the emergence of cellular life in real biological systems.[29] The aggregation process has been studied vis-à-vis the effect of external additives under normal circumstances.[24,25] However, in most of the cases, vesicular disruption or precipitation occurs with the increase in temperature that makes it very important to hunt for the systems where such phase transitions or disruptions can be avoided.[26−28]

The microstructural transitions and the morphology of the aggregates formed out of such transitions in a mixture of cationic and anionic surfactants are dependent on the nature and concentration of polar additives.[29] The addition of the additives to the systems has a critical disadvantage of complicating the systems by introducing the plethora of other "side interactions" which makes it difficult to tune the system to particular desirability.[20] A comprehensive report wherein both the transitions could be observed, that is, vesicle aggregation and VMTs induced by the temperature without the addition of any external additive, is still eluding the literature.

In this work, the catanionic surfactant system was realized in which we could observe both of these transitions as a function of temperature without involving additives. The studies have been carried out on a mixed surfactant system containing a cationic surfactant (CTAB) and surface-active ionic liquid (SAIL), based on SDS, that is, 1-butyl-3-methyl imidazolium dodecyl sulfate (bmimDS) as a function of temperature at various compositions. SAILs are an important class of ionic liquids that possess interesting physicochemical properties such as low vapor pressure, high thermal stability, wide liquidus range, and so forth.[4] than the conventional surfactant systems.[30] With the increase in temperature, the first transition was found to be a vesicle-to-aggregated vesicle transition at around 30 °C followed by a second transition involving vesicle-to-wormlike micelle transition concomitant with a large jump in the viscosity. Such systems have the potential to be used in a variety of applications ranging from biomedical to drug delivery application and as hydraulic fracturing fluids in enhanced oil recovery.[31] To the best of our knowledge, such a microstructural transition as a function of temperature in a single mixture of cationic and anionic surfactants has not been reported so far.[32]

2. RESULTS AND DISCUSSION

2.1. Physical appearance of the Surfactant Mixtures.

The physical appearance of the samples as a function of temperature exhibited a definite trend corresponding to a given mole fraction of CTAB (X_{CTAB}). Three distinct types of behaviors were observed corresponding to three ranges of X_{CTAB}, viz, X_{CTAB} = 0.25−0.5, X_{CTAB} = 0.55−0.65, and X_{CTAB} = 0.65−0.9 (see Figure 1 as a representative for each X_{CTAB} range). The solutions with X_{CTAB} = 0.1 and 0.2 remained slightly turbid in the whole range of temperature from 5 to 60 °C, indicating that no microstructural transitions take place in these solutions in this temperature range. However, in the case of the solutions with X_{CTAB} from 0.25 to 0.9, an interesting trend in the turbidity of the solutions is observed. In solutions with mole fractions 0.25 to 0.5 of CTAB, the turbidity remains unchanged as the temperature increases from 20 to 40−42 °C after which it (turbidity) shows a sharp decrease.

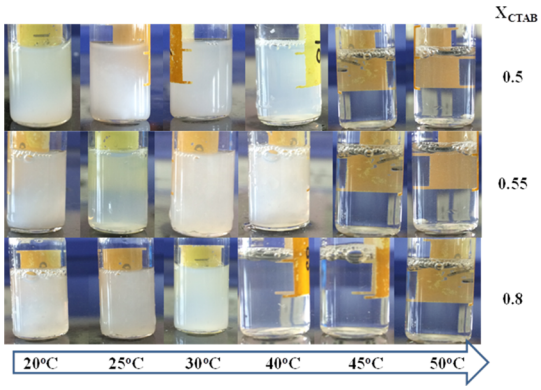

Figure 1. Physical appearance of three solutions as a function of temperature with mole fractions of CTAB as mentioned on the right side of each row.

Figure 2a shows the turbidity versus temperature plot for the solution with X_{CTAB} = 0.5 as a representative plot for X_{CTAB} ranging from 0.25 to 0.5. The abrupt change in the turbidity at about 40−42 °C signifies that some significant microstructural transition takes place at this temperature, most probably due to the transition from vesicle-to-micelle as the turbidity shows a decline in this temperature range which is characteristic of the micellar phase. Such a behavior has also been observed in the previous studies as well for the mixture of CTAB and SDS micellar systems.[14] In the case of solutions with mole fractions 0.55 to 0.65, the turbidity shows a different trend with the increase in temperature (Figure 2b).

As shown in the representative plot for X_{CTAB} = 0.55 in Figure 2b, the turbidity increases from mild values to significantly high values at around 30 °C, indicating that the smaller microstructures transit into some bigger microstructures in the solution. It is also evident from the visual inspection of the solution (Figure 1). From 30 to 40−42 °C, the turbidity remains almost constant after which it decreases abruptly at the higher temperatures, resulting in the clear solution as shown in the inset photographs of Figure 2b. This

https://doi.org/10.1021/acsomega.1c00469
ACS Omega 2021, 6, 11974−11987

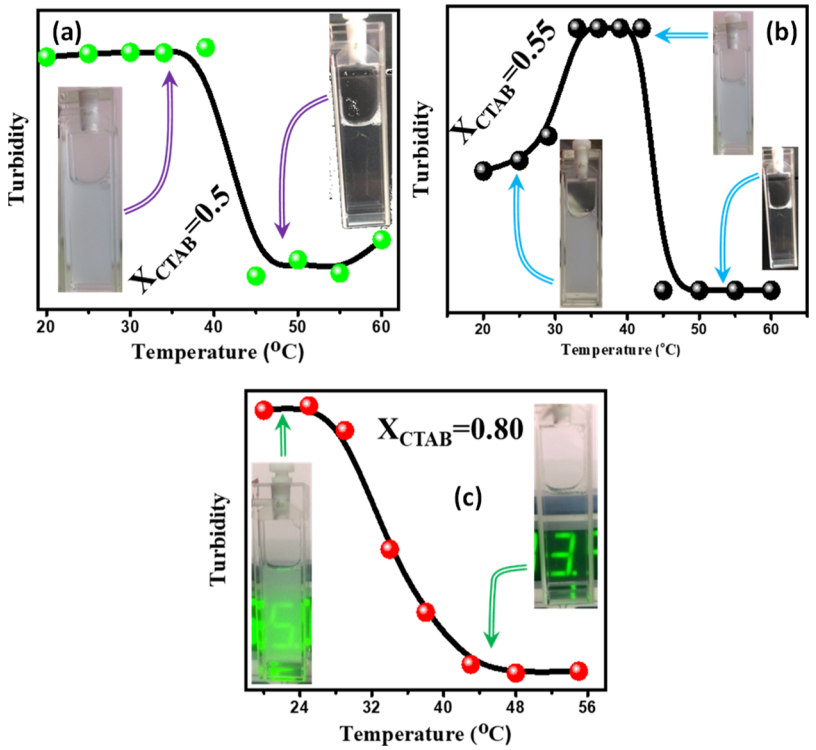

Figure 2. Plots showing the variation of turbidity as a function of temperature in (a) X_{CTAB} = 0.5, (b) X_{CTAB} = 0.55, and (c) X_{CTAB} = 0.8.

implies that with the increase in the mole fraction of CTAB, there is an occurrence of another transition at 30 °C in addition to the one at 40−42 °C. This transition at 30 °C in such solutions is ascribed to the vesicle aggregation process. A similar phenomenon has been reported by Yin et al.[28] in the case of a mixed surfactant system containing SDS and *n*-dodecyltributylammonium bromide (DTAB). The authors have reported the transition which is associated with the concomitant increase in the turbidity upto 30 °C. With the further increase in the mole fraction of CTAB, from 0.7 to 0.9, the turbidity decreases abruptly at 30 °C and then remains constant (Figure 2c, X_{CTAB} = 0.80 as the representative plot), implying only one transition at this temperature in such solutions. However, the transition at this temperature in these mole fractions is not the same as was observed in the X_{CTAB} of 0.55 to 0.65 at the same temperature because in these cases, the turbidity showed an increase in its value in contrast to the decrease in its value in the solutions with X_{CTAB} from 0.7 to 0.9. This could probably be the transition from vesicles to micelles in the case of higher-mole-fraction CTAB solutions.[32]

2.2. Rheological Characterization. *2.2.1. Dynamic Rheological Measurements.* To gain further insights into the temperature-induced transitions of the solutions studied, we have carried out the dynamic rheological experiments wherein we monitored the change in the storage modulus (G') and loss modulus (G'') with increasing temperature from 10 to 60 °C. Figure 3a shows the temperature dependence of G' and G'' for the solutions with X_{CTAB} from 0 to 0.4. From the figure, it is clear that the values of G' and G'' in X_{CTAB} 0.1 and 0.2 remain almost constant in the whole temperature range from 5 to 60 °C. In solutions of X_{CTAB} from 0.3 to 0.5, there is an abrupt jump in the values of G' and G'' at around 40−42 °C, the temperature which coincides very well with the transition temperature found by turbidity studies as discussed in the previous section. Since the rodlike micelles possess a higher elastic character than the vesicles, it can be concluded from the rheology and the turbidity measurements that the probable transition taking place at this temperature is a vesicle to rodlike micelle transition. In the case of solutions with X_{CTAB} = 0.55 to 0.65 (Figure 3b), two distinct transitions are observed in the temperature variant G' and G''measurements. At the first transition, which is observed at 30 °C, G' is more than G'' and both show a decrease in their values at about 30 °C. From 30 to 40−42 °C, the G' becomes less than G'' and both the values remain almost constant up to 40−42 °C after which both the values increase with again G' being greater than G''. The first transition at around 30 °C can be assigned to the vesicle aggregation process as being pointed out by the turbidity measurements. As mentioned earlier, this aggregation process has been observed by other authors as well in a different catanionic surfactant mixture.[28] The second transition at 40−42 °C most probably corresponds to the vesicle to rodlike micelle transition keeping into consideration the turbidity results. The two transitions observed in the dynamic rheological experiments do completely agree with the data obtained from the turbidity measurements. In the solutions with X_{CTAB} = 0.7 to 0.9, G' and G'' values show an abrupt decrease at only 30 °C (Figure 3c), showing only one transition at around 30 °C which is likely to be the vesicle (unilamellar) to small cylindrical/spherical micelle transition as also supported by the turbidity measurements. In summary, the results from the dynamic rheological measurements corroborate well with that of the turbidity measurements for all three ranges of mole fractions of CTAB.

2.2.2. Steady-State Rheological Measurements. In addition to the dynamic rheological measurements, we have also carried out the steady-state rheological experiments to further ascertain the position and nature of the transitions occurring as a function of temperature. Figure 4 shows the variation of viscosity (Pa s) with the changing shear rate (s^{-1}) for the

https://doi.org/10.1021/acsomega.1c00469
ACS Omega 2021, 6, 11974−11987

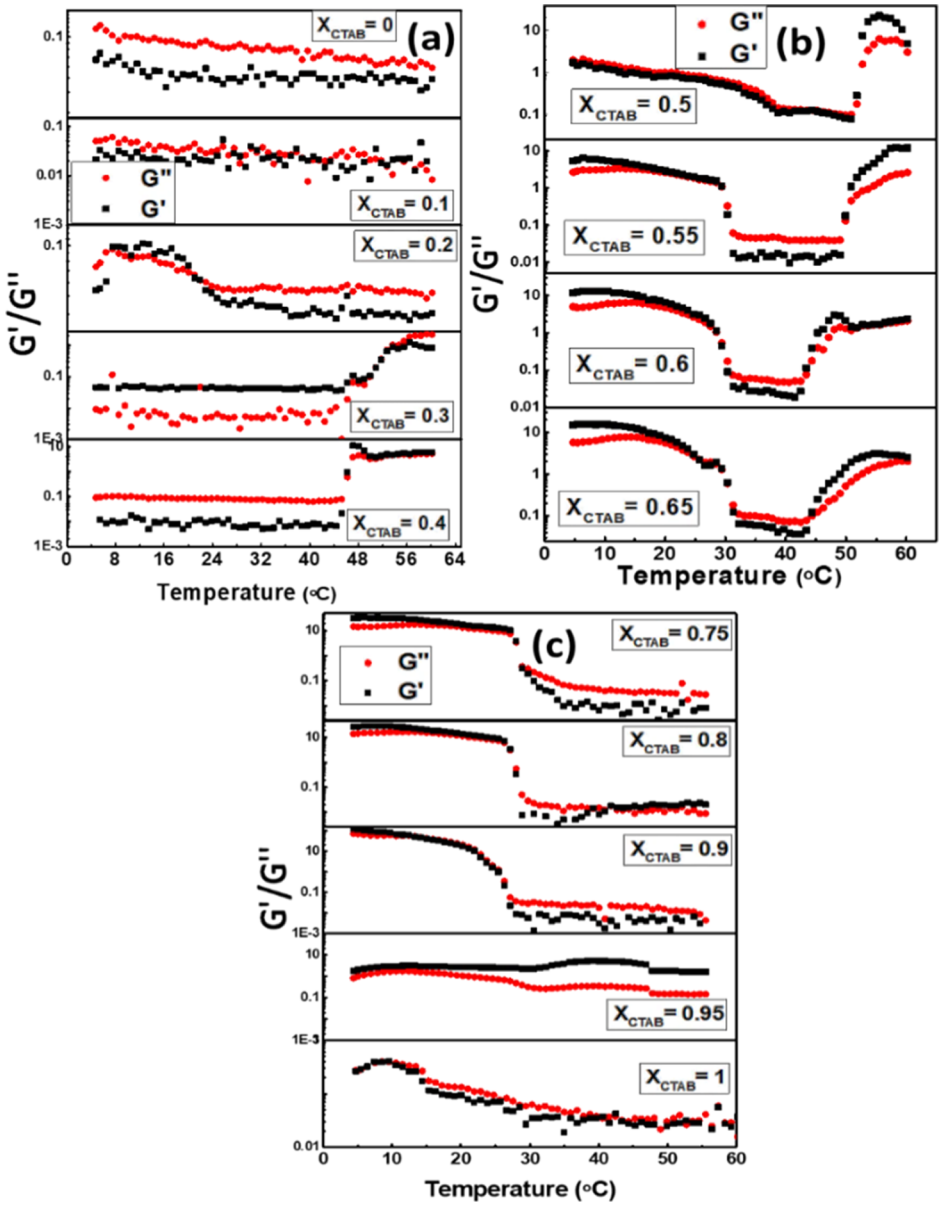

Figure 3. Temperature variation of G' and $G''$of the solutions with (a) X_{CTAB} = 0−0.5, (b) X_{CTAB} = 0.55−0.65, and (c) X_{CTAB} = 0.75−1.0.

X_{CTAB} = 0.5, 0.55, and 0.80 at different temperatures as a representative of three-mole fraction ranges. For the evaluation of the flow behavior of the solutions, we carried out the experiments to assess the viscoelastic behavior at three different temperatures of 10, 40, and 60 °C corresponding to the temperatures where the solutions are expected to exist in different microstructural forms. As can be seen from Figure 4a, the flow curve at 10 and 40 °C for X_{CTAB} = 0.5 describes the flow behavior which is a typical non-Newtonian fluid behavior. The flow curves show a small hump at the intermediate shear rates of about 1−10 s^{-1} which is characteristic of vesicular solutions,[33] thereby establishing the presence of vesicles in such a solution at temperatures up to 40 °C. It is pertinent to mention here that the solutions exhibit a viscous nature at low temperatures because of the decrease in the thermal energy of the system which renders high viscosity to the solutions. With the increase in temperature to 60 °C, the flow behavior changes significantly, exhibiting an increase in the low shear viscosity and the slight appearance of the viscosity plateau, which is indicative of the presence of entangled structures of rodlike micelles. Although the plateau is not prominent in this solution which is probably due to the difference in the mole fraction of two components, eventually leading to the disparate behavior in the low shear rates, due to their comparatively large size, rodlike micelles exhibit a slight resistance in their flow behavior when they are sheared slightly at low shear rates,[34] thereby exhibiting a viscosity plateau in their flow curves. On the other hand, the flow curves in the case of X_{CTAB} = 0.55 (Figure 4b) describe two different types of transitions, which are in complete agreement with the microstructural transitions inferred from the turbidity and dynamic rheological measurements. At 10 °C, the flow curve exhibits a hump at an intermediate value of shear rate, depicting the behavior typical of a vesicular solution.[33] It is worth mentioning here that at low temperatures, the solutions are more likely in a gel form, due to the high surfactant concentrations, which therefore imparts them the high viscosity at low shear rates. On increasing the temperature to 40 °C, which is a region of the

https://doi.org/10.1021/acsomega.1c00469
ACS Omega 2021, 6, 11974−11987

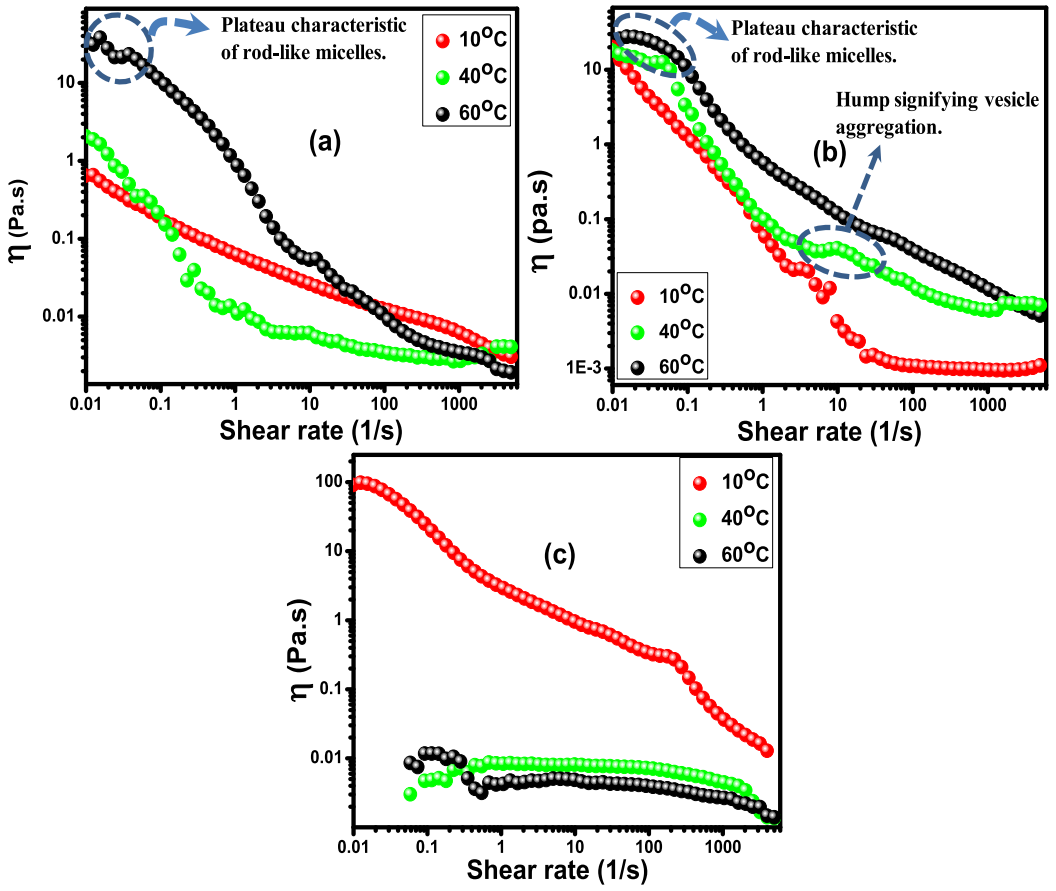

Figure 4. Prototype plots showing the variation of viscosity with the increase in the shear rate at various temperatures for different mole fractions of CTAB = (a) 0.5, (b) 0.55, and (c) 0.8.

aggregated vesicular region as deduced from dynamic rheological and turbidity measurements, the flow curve shows a more prominent hump at slightly intermediate shear rates (10−20 s^{-1}) than at 10 °C. The more prominent hump in the viscosity−shear rate profile may probably be because of the larger vesicles present in the solution as a result of the aggregation of smaller vesicles that would have taken place at 30 °C.[33] A further increase in the temperature of the solution to 60 °C changes the flow behavior to a significant extent. First, there is an appearance of a viscosity plateau at a low shear rate, which indicates the presence of entangled microstructures as pointed out earlier as well,[35] and second, the viscosity hump diminishes significantly at 60 °C. These two changes in the flow curves imply that at 60 °C, the microstructures in this solution change to rodshaped micelles from the aggregated vesicles. Finally, in the case of X_{CTAB} = 0.80 (Figure 4c), the flow behavior at 40 and 60 °C coincides with each other but is distinctively different from that at 10 °C, indicating two different types of microstructures present at 10 °C and 40/60 °C. Thus, the variation in the flow curve behavior is depictive of the only transition, from vesicles to short cylindrical/spherical micelles, which takes place at 30 °C. As this small cylindrical/spherical micelle solution is devoid of any extensive entanglements, low viscosity values at low shear rates and the Newtonian behavior are quite expected in contrast to the non-Newtonian behavior at 40 or 60 °C. From the abovementioned arguments, it is concluded that the rheological measurements are in complete agreement with the turbidity measurements as far as the nature of transitions is concerned. In order to further validate the occurrence of microstructural transitions in the catanionic mixture of CTAB and bmimDS, we have carried out the experiments using dynamic light scattering (DLS) and differential scanning calorimetry (DSC) techniques.

2.3. Differential Scanning Calorimetry. DSC has been extensively used to evaluate the transitions taking place in the microaggregate systems of soft self-assemblies as these transitions are often accompanied by the heat changes.[23,36,37] The heat effects are expected to arise because of the transfer of surfactant monomers to and from the vesicles/micelles, the enthalpies of which are positive to cause the endothermic effects.[23] Figure 5 sums up the DSC traces for the solutions with X_{CTAB} = 0.50, 0.55, and 0.80 as the representative samples from each region of the mole fraction of CTAB.

An endothermic peak with an outset at around 41 °C is observed in the X_{CTAB} = 0.5, which corresponds to the temperature at which vesicle to rodlike micelle transition occurs with an enthalpy change of around 3.63 J/g (Table 1). In the case of X_{CTAB} = 0.55, there are two endothermic peaks observed at 30 and 42 °C. The first peak at 30 °C signifies the transition corresponding to the vesicle aggregation process with an enthalpy change of about 3.00 J/g, and the peak at about 42 °C corresponds to the second transition of the vesicle to rodlike micelles with a higher enthalpy change (4.55 J/g) associated with it. For solution X_{CTAB} = 0.80, as expected, a single endothermic peak at around 30 °C has been observed, which has been ascribed to the vesicle to small cylindrical/spherical micelle transitions. It is pertinent to mention here

https://doi.org/10.1021/acsomega.1c00469
ACS Omega 2021, 6, 11974−11987

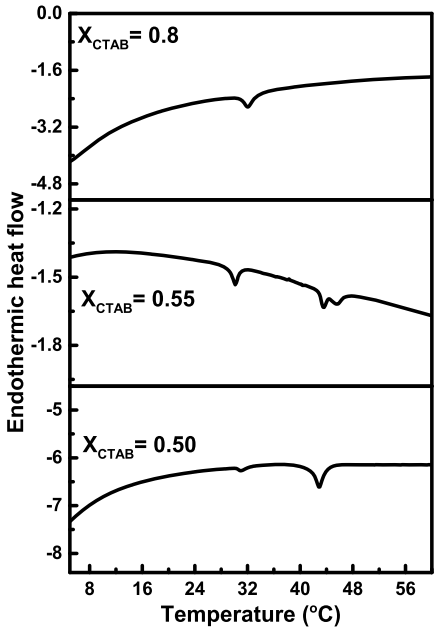

Figure 5. DSC plots for the solutions with the mole fraction of CTAB as mentioned in the legends of the graphs.

Table 1. Temperature of the Onset and Endset Temperatures Along with the Other Parameters Obtained from the DSC

X_{CTAB}	Onset transition temperature (°C)	Endset transition temperature (°C)	Peak temperature (°C)	Peak width (°C)	Enthalpy[a] (J/g)
0.50	41.26	43.22	42.84	1.96	3.63
0.55	29.18	30.99	30.20	1.81	3.003
	42.15	46.39	43.34	4.24	4.55
0.80	29.87	33.87	31.70	4.00	6.72

[a]Experimental error ≈±5%.

that the enthalpy change associated with this transition at this mole fraction is the highest of all the transitions. We opinionate that the enthalpy change, in this case, is due to the maximum possible structural organization (from vesicles to small cylindrical/spherical micelles) required to bring out this transition. Furthermore, the peak widths of all the transitions are proportional to the enthalpy changes associated with the microstructural transitions which are because the area of the peaks dictates the enthalpy changes accompanying such transitions. All the transition temperatures obtained for each composition studied are in complete agreement with the turbidity and rheological results.

2.4. Dynamic Light Scattering. DLS is a powerful technique for the determination of the size distribution of the microstructures involved in various transitions of different systems. To further authenticate the microstructural transitions involved in the mixed system of CTAB and bmimDS, we utilized the DLS measurements for the same three solutions which were used in the steady-state rheological experiments, to cover up all the three types of transitions involved in the solutions of different mole fractions of CTAB. To get a thorough and rational view of the microstructural transitions, we have carried out the DLS measurements at temperatures from 10 to 60 °C with various intervals. Figure 6 shows the size distribution plots of solutions with X_{CTAB} = 0.50, 0.55, and 0.80, at various temperatures. In X_{CTAB} = 0.50 (Figure 6a), at 20, 25, and 30 °C, the size distribution of the sample is around 150−200 nm, which shows the presence of microaggregates corresponding to vesicles. The size distribution remains almost the same on increasing the temperature up to about 40 °C above which the size distribution of the sample decreases drastically to around 25−35 nm, typical of the size of rod-shaped micelles.[30] On increasing the X_{CTAB} to 0.55 (Figure 6b), there was an increase in the size of the microstructures at around 30 °C and then a decrease after 40 °C. At temperatures from 10 to 30 °C, the size of the microaggregates ranges from 60 to 70 nm, which is a vesicular size, given that the solution is very much turbid in appearance at these temperatures. After 30 °C, the size distribution of the aggregates shows an abrupt jump to about 90−135 nm, indicating the formation/presence of bigger microaggregates in the solution. As the solution becomes much more turbid at this very temperature, the aggregation process of the smaller vesicles to larger vesicles is safe to be concluded. Afterward, the solution above 45 °C shows a decrease in the value of the diameter (40−50 nm) of the aggregates, which is consistent with the formation of rodlike micelles as pointed out also by the decrease in the turbidity of solution at this temperature. The solution with X_{CTAB} = 0.80 (Figure 6c) showed only one transition at 30 °C, wherein the size distribution of the microaggregates decreases drastically from 130−160 to 3−10 nm, typical of short cylindrical/spherical micelles. In the rheological and turbidity studies, the solution shows a decrease in the viscosity with a simultaneous decrease in the turbidity, pointing toward the vesicle to micelle transition. This transition from vesicles to smaller cylindrical/spherical micelles is well supported by the DLS measurements. To confirm the type of microstructures involved in the transitions, we have carried out the scattering experiments at various specified temperatures as discussed below.

2.5. Small-Angle Neutron Scattering. To have an insight into the type of microstructures involved in the transitions with varying temperatures, we have carried out the small-angle neutron scattering (SANS) measurements at different temperatures which fall within the different transition zones of three solutions (X_{CTAB} = 0.5, 0.55, and 0.8). The SANS spectra (Figure 7) of the studied mole fractions show very insignificant correlation peaks, a strong indication of the absence of interparticle interactions.[38] It is worth mentioning here that the scattering intensity at high Q values is indicative of the changes in the smallest dimensions of the microstructures, which, in this case, depends on the temperature of interest. The relative contributions of changes in the high- and low-Q scattering intensities at different temperatures have been taken into account by the appropriate model fitting, the accuracy of which was determined by the value of reduced Chi-square (χ^2). In X_{CTAB} = 0.5 solution, the SANS spectra display a similar behavior at temperatures of 20 and 35 °C, which indicates that the microstructures present at such temperatures are similar. Model fitting of the data revealed that the best fit for such a solution at these molefractions is the core−shell ellipsoid vesicle. To have better clarity and understanding of the shape and parameters of the microstructures, Scheme 1 depicts the shape and structure of the microstructures involved in the overall transformations as obtained from Sasview analysis. The calculated parameters, in this case, equatorial radius of the core ($R_{eq.\ core}$), and thickness of the shell at the equator ($thickness_{shell,\ eq.}$) are enlisted in Table 2. When the

https://doi.org/10.1021/acsomega.1c00469
ACS Omega 2021, 6, 11974−11987

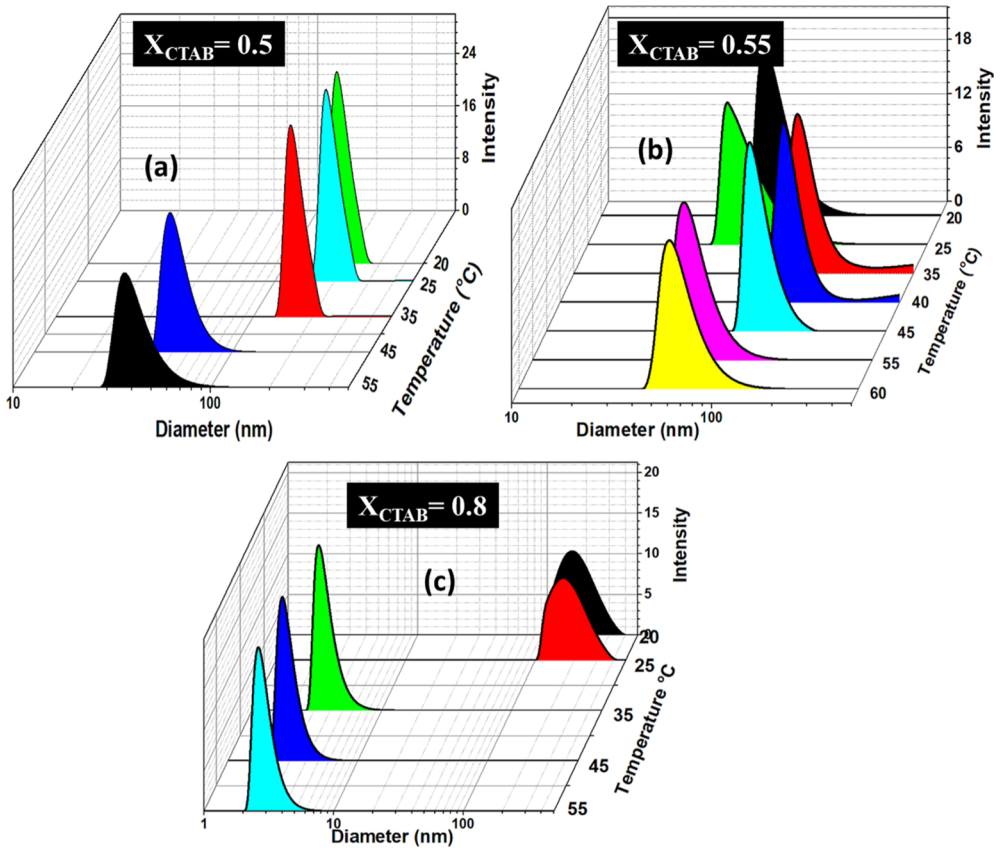

Figure 6. DLS plots of different mole fraction solutions of CTAB as a function of temperature: (a) X_{CTAB} = 0.5, (b) X_{CTAB} = 0.55, and (c) X_{CTAB} = 0.80.

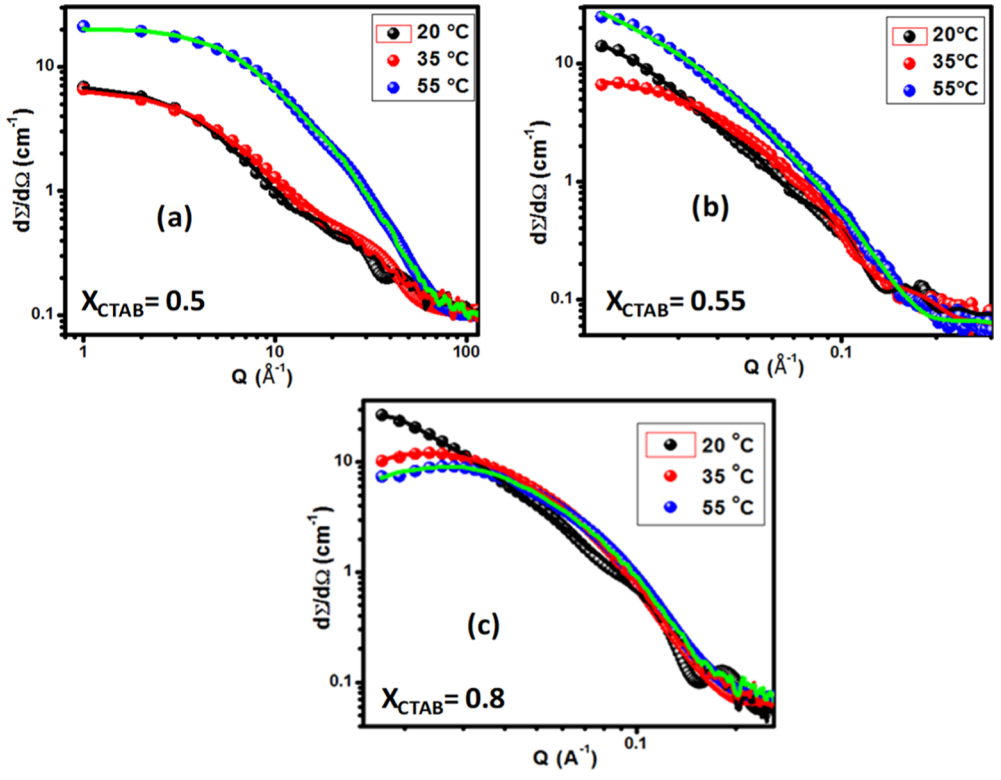

Figure 7. SANS spectra of the solutions at the different mole fractions of CTAB, X_{CTAB}, at different temperatures as mentioned for three mole fractions of solutions: (a) X_{CTAB} = 0.5, (b) X_{CTAB} = 0.55, and (c) X_{CTAB} = 0.8.

https://doi.org/10.1021/acsomega.1c00469
ACS Omega 2021, 6, 11974−11987

Scheme 1. Depiction of Different Microstructures Involved in the Microstructural Transformation

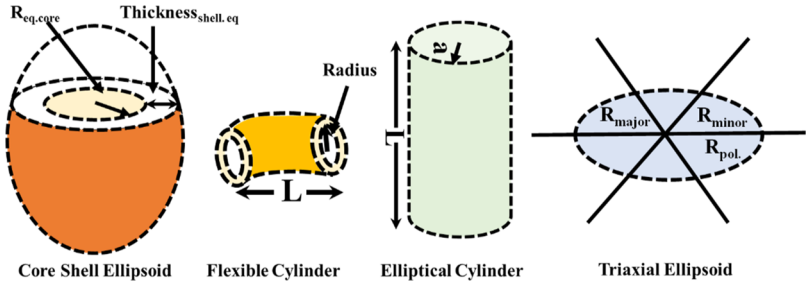

Table 2. SANS Parameters of the Solutions at Three Different Mole Fractions of CTAB at Different Temperatures

model		parameters		
X_{CTAB} = 0.50		$R_{eq,\ core}$ (Å)	$thickness_{shell,\ eq.}$ (Å)	χ^2
20 °C	core−shell ellipsoid	59.02	3.83	0.0025
35 °C	core−shell ellipsoid	22.02	17.31	0.0027
model		parameters		
X_{CTAB} = 0.50		radius minor (Å)	length (Å)	χ^2
55 °C	elliptical cylinder	16.19	151.7	0.003
model		parameters		
X_{CTAB} = 0.55		radius minor (Å)	length (Å)	χ^2
20 °C	core−shell ellipsoid	35.61	15.55	0.0029
model		parameters		
X_{CTAB} = 0.55		$R_{minor\ eq.}$[a] (Å)	$R_{major\ eq.}$[a] (Å)	$R_{pol.}$[a] (Å)	χ^2
35 °C	core−shell triaxial ellipsoid	77.29	17.31	18.9	0.0032
model		parameters		
X_{CTAB} = 0.55		radius minor (Å)	length (Å)	χ^2
55 °C	elliptical cylinder	16.21	186.82	0.0039
model		parameters		
X_{CTAB} = 0.8		$R_{eq.\ core}$ (Å)	$thickness_{core,\ eq.}$ (Å)	χ^2
20 °C	core−shell ellipsoid	30.89	14.8	0.003
model		parameters		
X_{CTAB} = 0.8		radius (Å)	length (Å)	χ^2
35 °C	flexible cylinder	17.31	77.29	0.0028
55 °C	flexible cylinder	16.21	64.82	0.0031

[a] $R_{minor\ eq.}$ = minor equatorial radius, $R_{major\ eq.}$ = major equatorial radius, and $R_{pol.}$ = polar radius.

temperature is increased to 55 °C, where we expect the presence of post-transitional (at 45 °C) microstructures, the low-Q scattering intensity shows a significant increase, which is an indication of the growth of micelles and increase in the intermicellar interactions. The model fitting data reveal that the transition at 45 °C has brought a microstructural change from core−shell ellipsoid vesicles to short flexible cylindrical micelles. With the increase in the mole fraction of CTAB to 0.55, the two transitions, at 30 and 45 °C, affected the SANS scattering intensity spectra significantly (Figure 7b). As can be seen, at a low temperature of 20 °C, the SANS data can be model fitted to core−shell ellipsoid structures with the parameters derived as shown in Table 2.

Interestingly, at 35 °C the SANS fitted data reveal the presence of triaxial core−shell ellipsoid microstructures, with the reduced χ^2 value of 0.0032. The triaxial structures in the solution at 35 °C are indicative of the aggregation of the core−shell ellipsoid microstructures at 30 °C, as discussed in earlier sections.

To confirm the presence of such aggregated vesicular structures, we fitted the data at this temperature to the core−shell ellipsoid model to cross-check the reliability of the data and we found that the regression of such a fit was around 0.06 which is 1 order of magnitude higher than the χ^2 value of the triaxial model (Figures S1−S3). Hence, the transition at 30 °C is the vesicle aggregation process wherein the smaller vesicles fuse together to form bigger vesicles with a triaxial core−shell ellipsoid geometry. With a further increase in the temperature of this solution (X_{CTAB} = 0.55), the triaxial vesicular structures transformed into elliptical cylindrical micelles as is evident from the increase in the low-Q scattering intensity of the SANS curve at 55 °C, indicative of the significant intermicellar interactions.[39] In the case of X_{CTAB} = 0.8, the solution at 20 °C temperature exhibits the scattering pattern which is befitting of a core−shell microstructure, as was the case in other mole-fraction solutions at this temperature. However, the increase in temperature to 35 °C and above produced a significant change in the scattering curves, especially in the low-Q region. The model-fitted data point toward the formation of flexible cylindrical structures, with a comparatively shorter length than the elliptically cylindrical micelles which are formed in CTAB mole fractions of 0.5 and 0.55 (Table 1). As a consequence of the presence of such shorter micelles, the viscosity of such solutions drops down at a transition temperature of 35 °C, as observed in rheological measurements.

2.6. Small-Angle X-ray Scattering. Small-angle X-ray scattering (SAXS) has been used quite extensively in the structure determination of lamellar microstructures.[40,41] Figure 8 shows the SAXS data profile of three solutions with mole fractions of CTAB, X_{CTAB} = 0.5, 0.55, and 0.80 at different temperatures as mentioned in the data plots. At X_{CTAB} = 0.5 (Figure 8a), the data plots below 45 °C temperatures exhibit a Braggs peak which is indicative of the presence of vesicles.[40] Only above 45 °C, these peaks disappear, which is marked by the transition from vesicles to rod-shaped micelles, in conformity with the abovediscussed results.

With X_{CTAB} increased to 0.55 (Figure 8b), the solution in which two transitions are observed, the Bragg peak still shows up; however, there is a noticeable shift in the peak maximum to lower q values at 40 °C, which has been assigned to the increase in the bilayer thickness by many workers.[35,42−45] The bilayer thickness "d" is measured by employing the data obtained from the plot of scattering intensity, $I(q)$ versus the scattering wave vector (q), and q is also related with the total scattering angle through the following equation

https://doi.org/10.1021/acsomega.1c00469
ACS Omega 2021, 6, 11974−11987

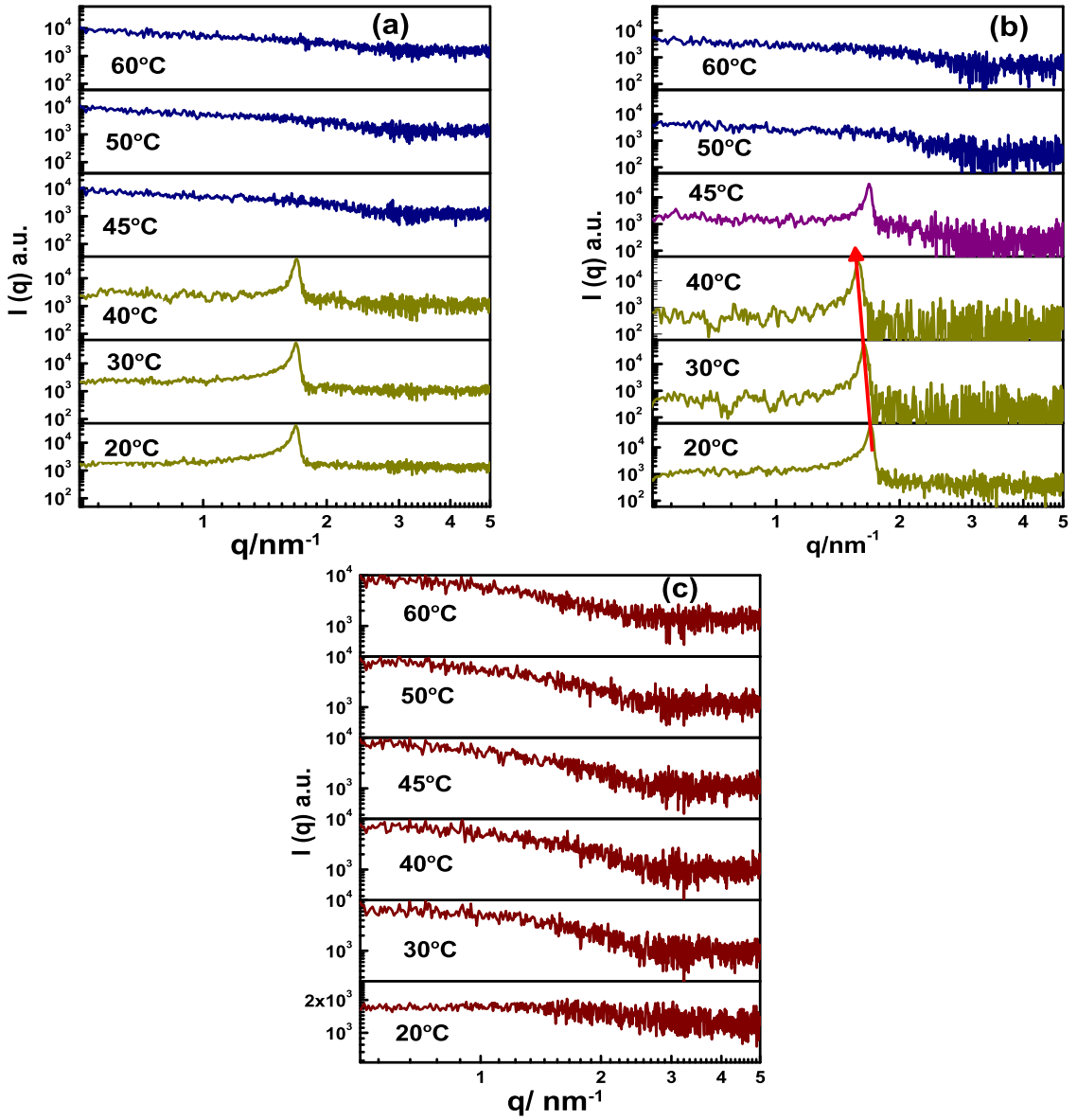

Figure 8. SAXS data profile of (a) X_{CTAB} = 0.5, (b) X_{CTAB} = 0.55, and (c) X_{CTAB} = 0.8 at different temperatures as mentioned in the data plots.

$$q = 2\pi/d = (4\pi/\lambda)\sin\theta/2 \quad (1)$$

At 20 °C, the plot of $I(q)$ versus (q) shows a maximum at 1.68 nm^{-1} which gives a bilayer thickness of ∼3.69 nm, while at 30 and 40 °C, the peaks have shifted to lower q values, resulting in an increase in "d" value to ∼3.78 and ∼3.9 nm, respectively, which signifies the aggregation of the micro-structures. However, with a further increase in temperature to 45 °C, the vesicles start to disintegrate as indicated by their lesser bilayer thickness values of ∼3.65 nm, which disappears with a further increase in temperature as is clear from the absence of the Bragg peak at such temperatures. It is pertinent to mention here that the increase in the bilayer thickness due to the aggregation process could result from the molecular rearrangements which take place when the bilayers of two or more vesicles fuse together. The phenomenon of vesicle aggregation has been ascribed to be taking place in two steps,[46,47] (1) docking of the bilayers of adjacent vesicles and (2) fusion of the docked bilayers via molecular rearrangements to form the fused vesicles. With a further increase in the X_{CTAB} to 0.8 (Figure 8c), the vesicles are formed below 20 and 30 °C; however, the absence of Bragg peaks in such solutions may be attributed to the lesser amounts of the bmimDS ions present, which leads to the absence of lamellar structures, as discussed in the next section.

To gain further insights into the microstructural transitions, the normalized Guinier approximation analysis of the data sets at low Q regions was carried out by plotting ln $I(Q)$ versus the Q^2 (Figure S4). The different slopes of the plots give us an indication of the presence of different microstructures at the temperature of interest[48] which can better be described in terms of the variation of radius of gyration (R_g) of different species present in the sample. The radius of gyration R_g of the different samples at different temperatures was obtained from the slope of the linear region of the Guinier analysis through the following equation

$$\ln I(Q) = \ln I_o - \frac{Q^2 R_g^{\ 2}}{3} \quad (2)$$

https://doi.org/10.1021/acsomega.1c00469
ACS Omega 2021, 6, 11974−11987

The R_g for the three solutions has been plotted as a function of temperature in Figure 9. From the figure, it can be seen that

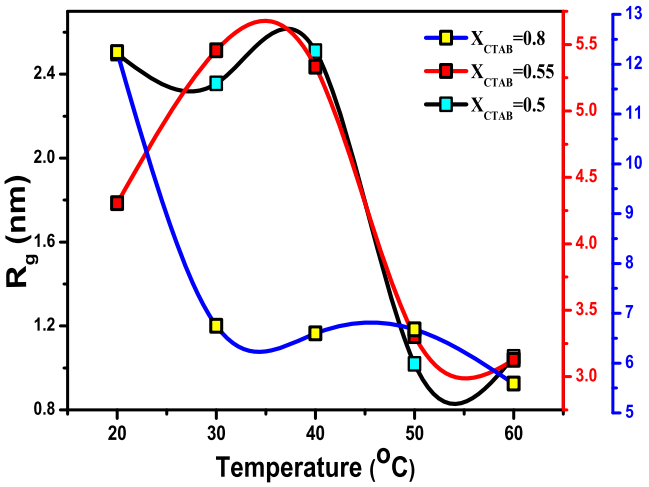

Figure 9. Variation of R_g as a function of temperature for the specified mole fraction solutions of the two surfactants.

the trends obtained so far from the preceding experimental techniques are also to be seen in the R_g values for different solutions. For example, in X_{CTAB} = 0.5, the R_g values exhibit an abrupt fall from 2.5 to 1.01 nm at 40 °C which is consistent with the observations deduced from the fact that such solutions exhibit microstructural transition at this temperature. X_{CTAB} = 0.55 exhibits the same bell-shaped trend in the R_g values as well, showing the first increase from 4.3 to 5.4 at 30 °C and then a decrease at around 42 °C to 3.3 nm. Finally, solution of X_{CTAB} = 0.8 exhibits the only significant decrease in R_g at 30 °C from 12.24 to 6.74 nm.

3. PROBABLE MECHANISM FOR THE TRANSITIONS IN THE MIXED SURFACTANT SYSTEMS

For the microstructural transitions observed in different mole fraction solutions of CTAB/bmimDS mixtures, an aplausible mechanism is put forth here based on the corollaries obtained from the various techniques as discussed above. The pure surfactant systems of CTAB and bmimDS exhibited the trends in their physicochemical properties, confirming the presence of micelles in such systems which remained unchanged when the temperature of solutions is increased from 10 to 60 °C. However, in the mixed state of two surfactants, different microstructures could be observed with an increase in temperature from 10 to 60 °C and these microstructural transitions exhibited different transitional behaviors vis-à-vis the nature of microstructures (Scheme 2). With the increase in mole fraction of CTAB, more specifically, X_{CTAB} = 0.3 to 0.5, the vesicles are transformed into the rodlike micelles, due to the desorption of $bmim^+$ from the vesicular interface. An increase in temperature of the solutions results in the desorption of $bmim^+$ ions from the vesicular interface which in turn leads to the increase in the head group area and decrease in the tail volume of the constituent ions.[19] Both these factors, viz., expansion of the head group area (cross-sectional area) and a decline in the inner volume of the tails, lead to the convergence into higher curvature aggregates typical of cylindrical micelles at a lower mole fraction of CTAB at higher temperatures as also reported by Davies et al.[19] (Scheme 3). A further increase in the mole fraction of CTAB (0.55 to 0.65) results in a different kind of morphological transition, with two of them taking place, one at 30 °C and the other one at 45 °C. The first transition at 30 °C is the vesicle aggregation transition wherein the comparatively smaller vesicles are transformed into the bigger vesicles. The increasingly higher amount of CTA^+ monomers at these mole fractions (0.55 to 0.65) result in the formation of a higher number of vesicles between CTA^+ and DS^- of bmimDS, as a consequence of which the process of vesicle aggregation is

Scheme 2. Schematic Representation of the Different Transitions Involved in Various Formulations with Changing Temperature

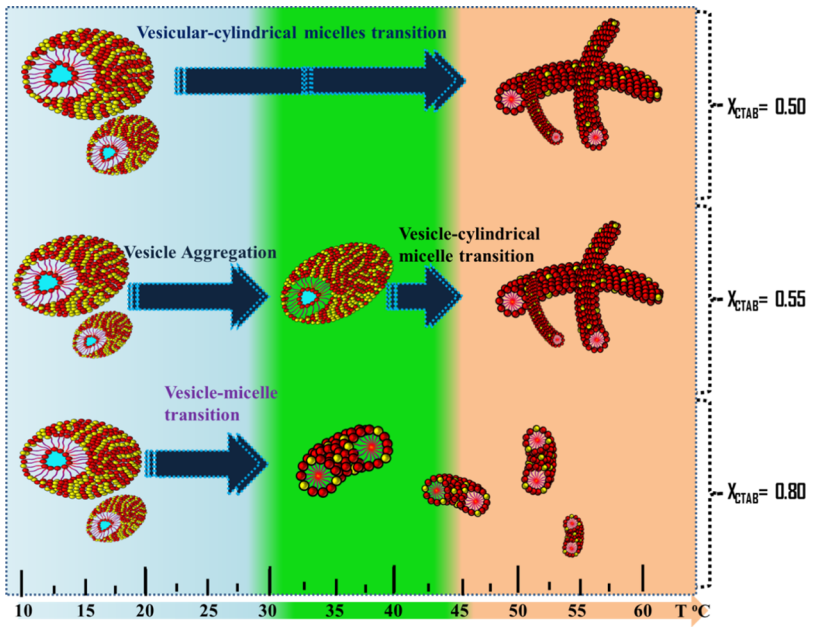

https://doi.org/10.1021/acsomega.1c00469
ACS Omega 2021, 6, 11974−11987

Scheme 3. Probable Mechanism of the Vesicular to Rodlike Micelle Transition Based on the Desorption of the $bmim^+$ Ion

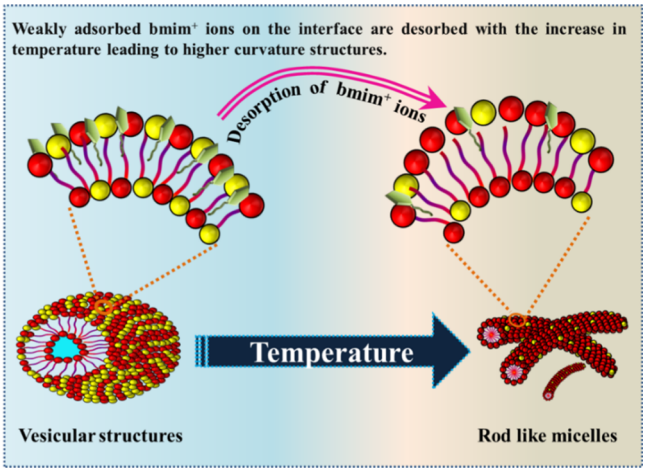

expedited. This is also supported by the fact that the vesicle aggregation process is not observed in the solutions with a lower mole fraction of CTAB (X_{CTAB} = 0.3−0.5) which could probably be because of the less number of vesicles present to have any observable effect on the aggregation process.[28] Moreover, due to the less charge on the vesicles in the mole fraction range of 0.55−0.65, owing to the electroneutrality, the process of vesicle aggregation is encouraged. It is pertinent to mention here that with an increase in temperature, the repulsive hydration forces are significantly decreased between the vesicles, which leads to their aggregation phenomenon. Besides the repulsive hydration forces, however, some authors have reported that the presence of hydrophobic moieties in the head group of some surfactants such as DTBAB plays an important role in bringing the vesicles together and hence aggregating them. However, in our case, the former force (decrease in the repulsive hydration forces) seems to be the predominant reason behind the aggregation phenomenon as we did not have any hydrophobic moiety in the head group of the surfactants, unlike DTBAB, which could have affected the transitions as we increased the temperature.[28] It may not be out of context to mention here that the interplay of both the forces, viz., decrease in the repulsive hydration forces and the decrease in the adsorption of $bmim^+$ ions, is held prominent in the mole fraction range of 0.5−0.65 for these two transitions to be observed simultaneously at two different temperatures (30 and 42 °C).

However, with a further increase in the amount of CTAB, that is, X_{CTAB} = 0.75 to 0.9, only one transition is observed at 30 °C, which is ascribed to be a vesicle-to-short flexible cylindrical micelle transition. It is worth mentioning here that with an increase in the amount of CTAB and the consequent decrease in the amount of bmimDS, the number of vesicles formed is relatively lesser (absence of Braggs peaks in the SAXS pattern), which could again explain the absence of the vesicle aggregation process in such solutions. Furthermore, the charge imbalance at the vesicular interface created due to the presence of more CTA^+ moieties could potentially lead to the increase in intervesicular repulsions, thereby hindering the aggregation phenomenon of vesicles. Nevertheless, the vesicles formed from CTAB and bmimDS at these mole fractions are disrupted to the mixed small cylindrical/spherical micelles with the increase in temperature.[14] The amount of $bmim^+$ ions at the vesicular interface (more positive surface due to the presence of a higher mole fraction of CTA^+ moieties) of these solutions is not high enough to affect the transition from vesicles to the cylindrical micelles due to the lack of ample screening of the head group charge.

4. EXPERIMENTAL SECTION

4.1. Chemicals Used. CTAB (99.8%) was a Sigma-Aldrich product that was used without further purifications. bmimDS was obtained from an ion−exchange reaction between SDS (Sigma-Aldrich; 98.9%) and bmimCl (Sigma-Aldrich; 98%) in water at 60 °C,[49] Scheme 4. Briefly, the equimolar solutions of SDS and bmimCl were mixed in a round-bottomed flask and heated at 60 °C with constant stirring for 24 h. The sample was obtained by fractional distillation of the mixture with dichloromethane (Himedia; 99.8%) by employing a separating funnel. The slightly yellow and viscous material (bmimDS) was washed several times with triple-distilled water before using it. The characterization of the sample was carried out by ^{1}HNMR (Figure S5) and tensiometric studies.

4.2. Preparation of Catanionic Surfactant Mixtures. The total concentration of the two surfactants CTAB and bmimDS in the mixture was fixed at 50 mM. The mole fraction

Scheme 4. Scheme Depicting the Synthesis of bmimDS and the Structures of the Surfactants Used in the Study

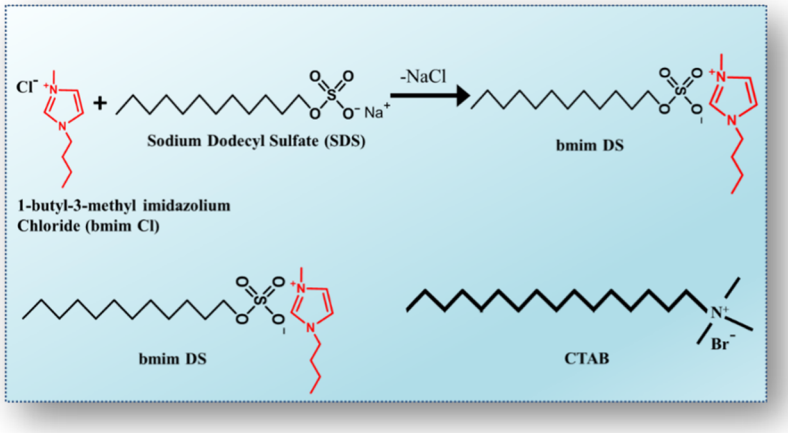

https://doi.org/10.1021/acsomega.1c00469
ACS Omega 2021, 6, 11974−11987

of CTAB in the mixture of surfactants was varied by mixing the appropriate volumes of the 50 mM stock solutions of each surfactant solution.

4.3. Phase Behavior Study and Turbidity Measurements. The phase behavior of the catanionic mixtures was followed visually and by measuring the turbidity of the solutions using Shimadzu UV−visible spectrophotometer model UV-1650 at a wavelength of 450 nm. The temperature of the mixed surfactant solutions was maintained using a Brookfield water circulating bath with a precision of ±0.1 °C.

4.4. Rheological Measurements. All the rheological measurements were performed on an Anton Paar modular compact rheometer (MCR 102) equipped with a Peltier-based temperature control system with an accuracy of ±0.01 °C. To study the variation of viscosity as a function of shear rate (0.1 to 1000 s^{-1}), cone and plate geometry with a diameter of 50 mm and cone angle of 1° was used. For the temperature sweep measurements, the temperature was varied from 5 to 60 °C with a heating rate of 2 °C/min at a constant angular frequency of 1 Hz and a strain of 0.5%. Silicone oil was applied during the temperature sweep measurements to avoid the evaporation of the sample at higher temperatures.

4.5. DLS Measurements. For determining the size of nanostructures formed as a function of temperature at various X_{CTAB}, DLS measurements were carried out using a Litesizer 500 (Anton Paar, Austria) at a scattering angle of 90°. The instrument is fitted with a Peltier temperature control apparatus which can vary the temperature with an accuracy of ±0.01 °C.

4.6. Differential Scanning Calorimetry. DSC experiments were performed using 61DSC-Pyris Diamond (PerkinElmer corp Norwalk, CT, USA). The indium standard was used for the calibration of the calorimeter. Samples were accurately weighed into aluminum DSC pans, and the pans were sealed tightly to avoid any water evaporation. The temperature was varied from 10 to 60 °C at a heating rate of 2°/min.

4.7. Small-Angle Neutron Scattering. SANS experiments were carried out using the SANS diffractometer at the Dhruva Reactor, Bhabha Atomic Research Centre, Trombay, India. The diffractometer makes use of a beryllium oxide filtered beam of mean wavelength (λ) 5.2 Å. The angular distribution of the scattered neutrons is recorded using a one-dimensional (1D) position-sensitive detector (PSD). The accessible wave vector transfer ($Q = 4\pi \sin \theta/\lambda$, where 2θ is the scattering angle) range of the diffractometer is 0.017−0.35 $Å^{-1}$. The PSD allows simultaneous recording of data over the full Q range. The samples were held in a quartz sample holder of 0.5 cm thickness. In all of the measurements, the temperature was kept as required for the system under consideration. The measured SANS data have been corrected and normalized to absolute units (as the cross section per unit volume), using standard procedures. Sasview version 5.0.3 was used to fit inbuilt different models to select the best fit model for the data.[50,51]

4.8. Small-Angle X-ray Scattering. SAXS experiments were performed in linear collimation in a modified Kratky camera (SAXSess Anton Paar, Austria) using Cu Kα as incident radiation (λ = 1.542 Å). The sample to detector distance was kept at 26.5 cm. The scattering intensities were collected for 1 h at the desired temperature on a two-dimensional position-sensitive imaging plate and integrated over a linear profile to convert into one-dimensional scattering data of scattering intensity $I(Q)$ versus scattering wave vector Q. Scattering data were corrected for the solvent (deionized water) to obtain the scattering intensity of the micelles in an arbitrary scale.

5. CONCLUSIONS

This work includes the study of microstructural transitions as a function of composition and temperature in a mixture of a conventional cationic surfactant, CTAB, and an anionic SAIL bmimDS. The formation and transformation of the microstructures have been evaluated with various techniques such as turbidity, rheology, DSC, DLS, SANS, and SAXS. The disparity in the microstructural evolution as a function of temperature has a steep dependence on the composition of the mixture which is a consequence of the difference in the number of ions present in a solution which in turn affects the balance of forces and leads to different types of microstructural transitions. In summary, the solutions with lower X_{CTAB} (X_{CTAB} = 0.1−0.5) exhibit only one transition at around 45 °C which has been evaluated to be a vesicle to rodlike micelle transition, while the solutions with X_{CTAB} = 0.55−0.65 exhibited two different types of transitions, first one at 30 °C and the second one at around 40−42 °C. The first transition at 30 °C was found to be a vesicle aggregation process, while the second one at 40−42 °C was found to be a vesicle to rodlike micelle transition. A further increase in the mole fraction of CTAB (X_{CTAB} = 0.65 to 0.9) resulted in only one transition, at 30 °C, which was recognized as a vesicle to short cylindrical/spherical micelle transition. The difference in the type of microstructures arises out of the changes in the balance of forces at the microstructure interface which is a consequence of the composition of the microstructure. A higher concentration of $bmim^+$ ions at lower X_{CTAB} solutions induces vesicle-to-cylindrical micelle transition owing to the effective screening of the head groups due to the intercalation of $bmim^+$ ions between the surfactant molecules. A further increase in the mole fraction of CTAB leads to a decrease in the surface charge of vesicles which augments the vesicle aggregation process at 30 °C in these mole fractions in addition to the transition at 42 °C which is a vesicle to cylindrical micelle transition. At a higher mole fraction of CTAB, the vesicles are again imbalanced in terms of surface charge, predominantly exhibiting a positive surface charge and hence decreasing the effective concentration of $bmim^+$ ions at the vesicular interface, as a result of which the transition arising due to the intercalation of $bmim^+$ ions, that is, vesicle-to-cylindrical transition vanishes. Instead, only one transition is observed, which is the vesicle-to-flexible micelles/short cylindrical micelles at 30 °C.

■ ASSOCIATED CONTENT

Supporting Information

The Supporting Information is available free of charge at https://pubs.acs.org/doi/10.1021/acsomega.1c00469.

Residual plots of SANS fit data, Guinier analysis plots of SANS data, and qNMR of the bmimDS surfactant to determine the purity (PDF)

■ AUTHOR INFORMATION

Corresponding Author

Aijaz Ahmad Dar − *Soft Matter Research Group, Department of Chemistry, University of Kashmir, Srinagar 190006,*

https://doi.org/10.1021/acsomega.1c00469
ACS Omega 2021, 6, 11974−11987

Jammu and Kashmir, India; orcid.org/0000-0003-1118-8566; Email: aijaz_n5@yahoo.co.in, aijazdar@kashmiruniversity.ac.in

Authors

Mohd Sajid Lone − *Soft Matter Research Group, Department of Chemistry, University of Kashmir, Srinagar 190006, Jammu and Kashmir, India*

Saima Afzal − *Soft Matter Research Group, Department of Chemistry, University of Kashmir, Srinagar 190006, Jammu and Kashmir, India*

Oyais Ahmad Chat − *Soft Matter Research Group, Department of Chemistry, University of Kashmir, Srinagar 190006, Jammu and Kashmir, India; Department of Chemistry, Government Degree College Pulwama, Pulwama 192301, Jammu and Kashmir, India;* orcid.org/0000-0003-4533-6459

Vinod Kumar Aswal − *Solid State Physics Division, Bhabha Atomic Research Centre, Mumbai 400 085, India;* orcid.org/0000-0002-2020-9026

Complete contact information is available at: https://pubs.acs.org/10.1021/acsomega.1c00469

Notes

The authors declare no competing financial interest.

■ ACKNOWLEDGMENTS

M.S.L. acknowledges the financial assistance by UGC as UGC SRF, and S.A. acknowledges financial assistance by CSIR as CSIR-SRF. A.A.D. acknowledges DST and UGC, India, for providing funds under FIST level-1 and SAP DRS-1, respectively, to the Department of Chemistry, University of Kashmir. A.A.D. also acknowledges MHRD, India, for providing funds under RUSA Scheme 2.0 that augmented this work. We are thankful to Anton Paar, India, for the SAXS experiments and analysis.

■ REFERENCES

(1) Yada, S.; Shimosegawa, H.; Fujita, H.; Yamada, M.; Matsue, Y.; Yoshimura, T. Microstructural Characterization of Foam Formed by a Hydroxy Group-Containing Amino Acid Surfactant Using Small-Angle Neutron Scattering. *Langmuir* **2020**, *36*, 7808−7813.

(2) Lone, M. S.; Afzal, S.; Nazir, N.; Dutta, R.; Dar, A. A. Excimer Based FRET between Non-FRET Pair Flourophores Aided by the Aromatic Moiety of Anionic Surfactants: An Experimental Observation. *J. Mol. Liq.* **2019**, *277*, 84−92.

(3) Lone, M. S.; Bhat, P. A.; Afzal, S.; Chat, O. A.; Dar, A. A. Energy Transduction through FRET in Self-Assembled Soft Nanostructures Based on Surfactants/Polymers: Current Scenario and Prospects. *Soft Matter* **2021**, *17*, 425−446.

(4) Mamusa, M.; Arroyo, M. C.; Fratini, E.; Giorgi, R.; Baglioni, P.; Ugo, C.; Fiorentino, S. Nonaqueous Microemulsion in the Bmim Tf2N/Brij 30/n-Nonane System: Structural Investigation and Application as Gold Nanoparticle Microreactor. *Langmuir* **2018**, *34*, 12609−12618.

(5) Xia, Y.; Dong, L.; Jin, Y.; Wang, S.; Yan, L.; Yin, S.; Zhou, S.; Song, B. Water-soluble nano-fluorogens fabricated by self-assembly of bolaamphiphiles bearing AIE moieties: towards application in cell imaging. *J. Mater. Chem. B* **2015**, *3*, 491−497.

(6) Rubingh, D. N. *Solution Chemistry of Surfactants*; Plenum press: New York, 1979.

(7) Holland, P. M.; Rubingh, D. N. Nonideal Multicomponent Mixed Micelle Model. *J. Phys. Chem.* **1983**, *87*, 1984−1990.

(8) Söderman, O.; Herrington, K. L.; Kaler, E. W.; Miller, D. D. Transition from Micelles to Vesicles in Aqueous Mixtures of Anionic and Cationic Surfactants. *Langmuir* **1997**, *13*, 5531−5538.

(9) Yin, H.; Huang, J.; Lin, Y.; Zhang, Y.; Qiu, S.; Ye, J. Heating-Induced Micelle to Vesicle Transition in the Cationic−Anionic Surfactant Systems: Comprehensive Study and Understanding. *J. Phys. Chem. B* **2005**, *109*, 4104−4110.

(10) Dutta, R.; Ghosh, M.; Pyne, A.; Sarkar, N. Insight into the Dynamics of Different Fluorophores in the Interior of Aerosol OT Lamellar Structures in the Presence of Sugars: From Picosecond-to-Femtosecond Study. *J. Phys. Chem. B* **2019**, *123*, 117−129.

(11) Sachin Krishnan, T. V.; Das, S. L.; Kumar, P. B. S. Transition from Curvature Sensing to Generation in a Vesicle Driven by Protein Binding Strength and Membrane Tension. *Soft Matter* **2019**, *15*, 2071−2080.

(12) Mokhtary, P.; Javan, B.; Sharbatkhari, M.; Soltani, A.; Erfani-Moghadam, V. Cationic Vesicles for Efficient ShRNA Transfection in the MCF-7 Breast Cancer Cell Line. *Int. J. Nanomed.* **2018**, *13*, 7107−7121.

(13) Wang, H.; Tan, B.; Zhang, H.; Wang, J. pH triggered self-assembly structural transition of ionic liquids in aqueous solutions: smart use of pH-responsive additives. *RSC Adv.* **2015**, *5*, 65583−65590.

(14) Rajkhowa, S.; Mahiuddin, S.; Dey, J.; Kumar, S.; Aswal, V. K.; Biswas, R.; Kohlbrecher, J.; Ismail, K. The Effect of Temperature, Composition and Alcohols on the Microstructures of Catanionic Mixtures of Sodium Dodecylsulfate and Cetyltrimethylammonium Bromide in Water. *Soft Matter* **2017**, *13*, 3556−3567.

(15) Afzal, S.; Lone, M. S.; Maswal, M.; Dar, A. A. Modulation of Surface Tension and Rheological Behavior of Methyl Cellulose − Amino Acid Based Surfactant Mixture by Hydrophobic Drug Rifampicin: An Insight into Drug Stabilization and PH-Responsive Release. *J. Mol. Liq.* **2020**, *319*, 114353.

(16) Yang, Y.; Dong, J.; Li, X. Micelle to Vesicle Transitions of N-Dodecyl-1 , x -Diaminoalkanes: Effects of PH , Temperature and Salt. *J. Colloid Interface Sci.* **2012**, *380*, 83−89.

(17) Fernyhough, C.; Ryan, A. J.; Battaglia, G. pH controlled assembly of a polybutadiene-poly(methacrylic acid) copolymer in water: packing considerations and kinetic limitations. *Soft Matter* **2009**, *5*, 1674−1682.

(18) Jiang, L.; Wang, K.; Ke, F.; Liang, D.; Huang, J. Endowing Catanionic Surfactant Vesicles with Dual Responsive Abilities via a Noncovalent Strategy: Introduction of a Responser, Sodium Cholate. *Soft Matter* **2009**, *5*, 599−606.

(19) Davies, T. S.; Ketner, A. M.; Raghavan, S. R. Self-Assembly of Surfactant Vesicles That Transform into Viscoelastic Wormlike Micelles upon Heating. *J. Am. Chem. Soc.* **2006**, *128*, 6669.

(20) Silva, B. F. B.; Marques, E. F.; Olsson, U. Unusual Vesicle−Micelle Transitions in a Salt-Free Catanionic Surfactant: Temperature and Concentration Effects. *Langmuir* **2008**, *24*, 10746−10754.

(21) Mitra, S.; Sharma, V. K.; Garcia-Sakai, V.; Orecchini, A.; Seydel, T.; Johnson, M.; Mukhopadhyay, R. Enhancement of Lateral Diffusion in Catanionic Vesicles during Multilamellar-to-Unilamellar Transition. *J. Phys. Chem. B* **2016**, *120*, 3777−3784.

(22) Abdel-Rahem, R.; Hoffmann, H. Novel Viscoelastic Systems from Cationic Surfactants and Hydrophobic Counter-Ions: Influence of Surfactant Chain Length. *J. Colloid Interface Sci.* **2007**, *312*, 146−155.

(23) Majhi, P. R.; Blume, A. Temperature-Induced Micelle-Vesicle Transitions in DMPC−SDS and DMPC−DTAB Mixtures Studied by Calorimetry and Dynamic Light Scattering. *J. Phys. Chem. B* **2002**, *106*, 10753−10763.

(24) Minami, H.; Inoue, T. Aggregation of Dipalmitoylphosphatidylcholine Vesicles Induced by Some Metal Ions with High Activity for Hydrolysis. *Langmuir* **1999**, *15*, 6643−6651.

(25) Walker, S. A.; Zasadzinski, J. A. Electrostatic Control of Spontaneous Vesicle Aggregation. *Langmuir* **1997**, *13*, 5076−5081.

(26) Wilkinson, D. A.; Nagle, J. F.; Knight, C. G. *Liposomes*; Elsevier: Amsterdam, 1981.

(27) Ansell, G. B.; Hawthorne, J. N. *Phospholipids*; Elsevier: Amsterdam, 1982.
(28) Yin, H.; Huang, J.; Gao, Y.; Fu, H. Temperature-Controlled Vesicle Aggregation in the Mixed System of Sodium n -Dodecyl Sulfate / n -Dodecyltributylammonium Bromide. *Langmuir* **2005**, *21*, 2656−2659.
(29) Roy, A.; Dutta, R.; Banerjee, P.; Kundu, S.; Sarkar, N. 5-Methyl Salicylic Acid-Induced Thermo Responsive Reversible Transition in Surface Active Ionic Liquid Assemblies: A Spectroscopic Approach. *Langmuir* **2016**, *32*, 7127−7137.
(30) Chat, O. A.; Maswal, M.; Hassan, P. A.; Aswal, V. K.; Rather, G. M.; Dar, A. A. Effect of Mixed Micellization on Dimensions of 1-Butyl-3-Methylimidazolium Dodecylsulfate Micelles in Presence of Electrolytes. *Colloids Surf., A* **2015**, *484*, 498−507.
(31) Castro Dantas, T.; Santanna, V. C.; Dantas Neto, A. A.; Barros Neto, E. L.; Alencar Moura, M. C. P. Rheological Properties of a New Surfactant-Based Fracturing Gel. *Colloids Surf., A* **2003**, *225*, 129−135.
(32) Ghosh, S.; Ghatak, C.; Banerjee, C.; Mandal, S.; Kuchlyan, J.; Sarkar, N. Spontaneous Transition of Micelle−Vesicle−Micelle in a Mixture of Cationic Surfactant and Anionic Surfactant-like Ionic Liquid: A Pure Nonlipid Small Unilamellar Vesicular Template Used for Solvent and Rotational Relaxation Study. *Langmuir* **2013**, *29*, 10066−10076.
(33) Ashraf, U.; Chat, O. A.; Maswal, M.; Jabeen, S.; Dar, A. A. An Investigation of Pluronic P123−Sodium Cholate Mixed System: Micellization, Gelation and Encapsulation Behavior. *RSC Adv.* **2015**, *5*, 83608−83618.
(34) Lone, M. S.; Bhat, P. A.; Shah, R. A.; Chat, O. A.; Dar, A. A. A Green PH-Switchable Amino Acid Based Smart Wormlike Micellar System for Efficient and Controlled Drug Delivery. *ChemistrySelect* **2017**, *2*, 1144−1148.
(35) Assaker, K.; Carteret, C.; Durand, P.; Aranda, L.; Stébé, M. J.; Blin, J. L.; Cnrs, L.; Cnrs, L.; Cnrs, L.; Cnrs, L. Hydrothermal Stability of Ordered Surfactant-Templated Titania. *J. Phys. Chem. C* **2013**, *117*, 16500−16508.
(36) Yin, H.; Zhou, Z.; Huang, J.; Zheng, R.; Zhang, Y. Temperature-Induced Micelle to Vesicle Transition in the Sodium Dodecylsulfate/Dodecyltriethylammonium Bromide System. *Angew. Chem., Int. Ed.* **2003**, *42*, 2188−2191.
(37) Bergsma, M.; Fielden, M. L.; Engberts, J. B. F. N. pH-Dependent Aggregation Behavior of a Sugar-Amine Gemini Surfactant in Water: Vesicles, Micelles, and Monolayers of Hexane-1,6-bis(hexadecyl-1′-deoxyglucitylamine). *J. Colloid Interface Sci.* **2001**, *243*, 491−495.
(38) Bhattacharjee, J.; Aswal, V. K.; Hassan, P. A.; Pamu, R.; Narayanan, J.; Bellare, J. Structural Evolution in Catanionic Mixtures of Cetylpyridinium Chloride and Sodium Deoxycholate. *Soft Matter* **2012**, *8*, 10130−10140.
(39) Han, C.; Guo, Y.; Chen, X.; Yao, M.; Zhang, Y.; Zhang, Q.; Wei, X. Phase Behaviour and Temperature-Responsive Properties of a Gemini Surfactant/Brij-30/Water System. *Soft Matter* **2017**, *13*, 1171−1181.
(40) Andreozzi, P.; Funari, S. S.; La Mesa, C.; Mariani, P.; Ortore, M. G.; Sinibaldi, R.; Spinozzi, F. Multi- to Unilamellar Transitions in Catanionic Vesicles. *J. Phys. Chem. B* **2010**, *114*, 8056−8060.
(41) Dutta, R.; Ghosh, M.; Pyne, A.; Sarkar, N. Insight into the Dynamics of Different Fluorophores in the Interior of Aerosol OT Lamellar Structures in the Presence of Sugars: From Picosecond-to-Femtosecond Study. *J. Phys. Chem. B* **2019**, *123*, 117.
(42) Demé, B.; Dubois, M.; Gulik-Krzywicki, T.; Zemb, T. Giant Collective Fluctuations of Charged Membranes at the Lamellar-to-Vesicle Unbinding Transition. 1. Characterization of a New Lipid Morphology by SANS, SAXS, and Electron Microscopy. *Langmuir* **2002**, *18*, 997−1004.
(43) Kiselev, M. A.; Lesieur, P.; Kisselev, A. M.; Lombardo, D.; Killany, M.; Lesieur, S. Sucrose Solutions as Prospective Medium to Study the Vesicle Structure: SAXS and SANS Study. *J. Alloys Compd.* **2001**, *328*, 71−76.
(44) Chu, X.; Xing, P.; Li, S.; Ma, M.; Hao, A. Inorganic Salt-Tuned Multiple Self-Assemblies of Supramolecular β-Cyclodextrin Gel. *Colloids Surf., A* **2014**, *461*, 11−17.
(45) Bhadani, A.; Okano, T.; Ogura, T.; Misono, T.; Sakai, K.; Abe, M.; Sakai, H. Structural features and surfactant properties of core-shell type micellar aggregates formed by gemini piperidinium surfactants. *Colloids Surf., A* **2016**, *494*, 147−155.
(46) Komorowski, K.; Schaeper, J.; Sztucki, M.; Sharpnack, L.; Brehm, G.; Köster, S.; Salditt, T. Vesicle Adhesion in the Electrostatic Strong-Coupling Regime Studied by Time-Resolved Small-Angle X-Ray Scattering. *Soft Matter* **2020**, *16*, 4142−4154.
(47) Komorowski, K.; Salditt, A.; Xu, Y.; Yavuz, H.; Brennich, M.; Jahn, R.; Salditt, T. Vesicle Adhesion and Fusion Studied by Small-Angle X-Ray Scattering. *Biophys. J.* **2018**, *114*, 1908−1920.
(48) Albert, S. K.; Sivakumar, I.; Golla, M.; Thelu, H. V. P.; Krishnan, N.; Libin, K. L. J.; Varghese, R. DNA-Decorated Two-Dimensional Crystalline Nanosheets. *J. Am. Chem. Soc.* **2017**, *139*, 17799−17802.
(49) Rather, M. A.; Rather, G. M.; Pandit, S. A.; Bhat, S. A.; Bhat, M. A. Determination of cmc of imidazolium based surface active ionic liquids through probe-less UV-vis spectrophotometry. *Talanta* **2015**, *131*, 55−58.
(50) Sanchez-Fernandez, A.; Leung, A. E.; Kelley, E. G.; Jackson, A. J. Complex by Design: Hydrotrope-Induced Micellar Growth in Deep Eutectic Solvents. *J. Colloid Interface Sci.* **2021**, *581*, 292−298.
(51) Hallett, J. E.; Grillo, I.; Smith, G. N. A Neutron Scattering Study of the Structure of Poly(Dimethylsiloxane)-Stabilized Poly-(Methyl Methacrylate) (PDMS−PMMA) Latexes in Dodecane. *Langmuir* **2020**, *36*, 2071−2081.

https://doi.org/10.1021/acsomega.1c00469
ACS Omega 2021, 6, 11974−11987